Biochimica et Biophysica Acta, 547 (1979) 484—501

BBA 47725

THE ORIENTATION OF THE PRIMARY DONOR IN BACTERIAL PHOTOSYNTHESIS

HARRY A. FRANK, RICHARD FRIESNER, JOHN A. NAIRN, G. CHARLES DISMUKES * and KENNETH SAUER

Laboratory of Chemical Biodynamics, Lawrence Berkeley Laboratory and Department of Chemistry, University of California, Berkeley, CA 94720 (U.S.A.)

(Received November 29th, 1978)

Key words: Bacterial photosynthesis; Triplet state; Reaction center; (EPR)

Summary

The triplet state EPR spectra of magnetically aligned whole cells of *Rhodopseudomonas viridis* and *Rhodopseudomonas palustris* display a marked dependence on the orientation of the static EPR field with respect to the alignment field direction. This observation implies that the primary donor species on which the triplets are localized are ordered within the membranes. We have developed a theoretical model for the system to enable calculation of the orientation of the magnetic axes of the primary donor species with respect to the membranes in which they reside. The triplet state spectra are generated by an ensemble of partially ordered magnetic systems and a computer simulation of the experimental results. The triplet orientation is very similar for the two organisms studied, where one axis lies predominantly in the plane of the membrane and the other two axes have approximately equal projections onto the normal to the membrane.

Introduction

Electron paramagnetic resonance (EPR) techniques have been used extensively in the study of triplet states in photosynthetic bacteria [1]. Experiments performed at zero field, and at high field, have focused on the triplet state as a probe into the structure of the reaction center [2,3] and as an indicator in redox titrations of the various components involved in the primary light reactions of bacterial photosynthesis [4—6].

* Present address: Frick Chemical Laboratory, Princeton University, Princeton, NJ 08540, U.S.A.

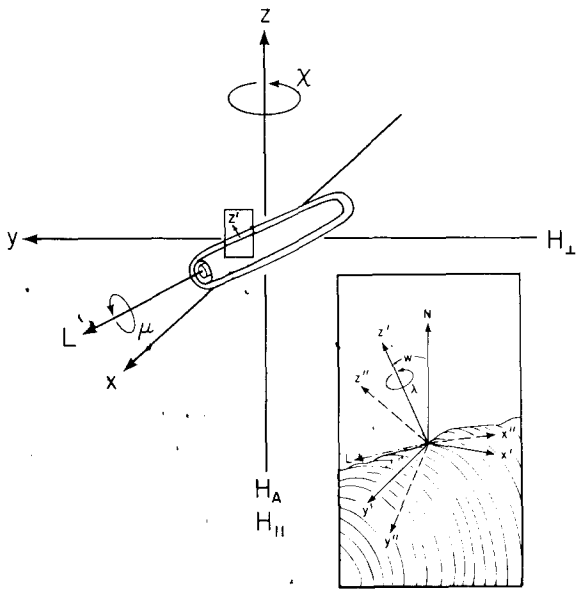

Fig. 1. Axis system and symmetry operation definitions. x, y and z define the laboratory axis system; x', y' and z' the intermediate axis system; x'', y'' and z'' the principal magnetic axis system. L is the long axis direction of the cell. χ, ν and λ are rotations about the indicated axes. H_A is the alignment field direction, and $H_\parallel$ and $H_\perp$ show the static EPR field directions used in the present experiments. Insert displays a section of the cylindrical membrane surface. The wobble angle, w, is defined as the angle between the membrane normal, z', and the perfect cylinder normal, N, (i.e. $N \perp L$).

The primary donor (designated P) in bacterial photosynthesis is a dimeric bacteriochlorophyll species [4,7—9]. There is strong evidence that the triplet state readily observed in various photosynthetic bacterial organisms belongs to this dimer [10] but is not part of the main pathway leading to photosynthesis [11]. This triplet state forms as the result of a radical pair recombination reaction that occurs between the oxidized primary donor and a reduced initial acceptor (labeled I). This happens when the electron flow has been blocked at a position immediately following I [6,11].

In this paper we consider the triplet states of two species of photosynthetic bacteria, *Rhodopseudomonas viridis* and *Rhodopseudomonas palustris* *. Both of these bacteria are prolate ellipsoidal organisms with highly ordered (cylindrical) internal membrane structures [12—14] (see Fig. 1). Reaction center particles which contain the primary donor are dispersed throughout these membranes. Electron microscope studies suggest that there is some degree of ordering of these particles in the membranes [12].

These bacterial organisms tend to align with their longitudinal axis perpendicular to an applied strong magnetic field [15,16]. This occurs in whole cells as the result of an induced diamagnetic moment within the membrane structures [15]. Recently, Paillotin et al. [16], using linear dichroism and photo-

* *Rps. palustris* differs from *Rps. viridis* in its pigmentation. *Rps. viridis* is a bacteriochlorophyll *b*-containing organism, whereas *Rps. palustris* has bacteriochlorophyll *a* as its major pigment.

selection techniques on magnetically aligned *Rps. viridis* cells have observed an orientation of the reaction center complexes within the bacterial membranes and have concluded that the primary donor resides in a fixed geometric relation to the membranes [16]. Two transition moments of the primary donor centered at 970 nm and 850 nm have been calculated to lie parallel to and at an angle greater than 55° to the membrane planes, respectively. Characterization of the two other bacteriochlorophyll molecules in the reaction center of *Rps. viridis* using this technique revealed that they are also coherently arranged.

In the present work we present a triplet state EPR study complementary to the afore mentioned linear dichroism investigation. We have magnetically aligned whole cells of *Rps. viridis* and *Rps. palustris* and studied their triplet state properties using a light modulation technique. By positioning the sample so that the static EPR field is either parallel or perpendicular to the alignment field direction, an orientation effect on the triplet signals is observed. From a knowledge of the distribution of the magnetically aligned cells and their internal membrane structure, we are able to calculate the projections that the triplet magnetic axes make with respect to the normal to the membranes.

Our approach is to construct a computer model that treats the sample of aligned bacterial organisms as an ensemble of partially ordered triplet states. An orientational distribution function that describes the manner and the degree of the system ordering is derived and used in simulating the observed spectra. In addition to the orientation information, zero-field splitting parameters and relative intersystem crossing rate constants for the triplet states are calculated.

Materials and Methods

Rps. viridis cells were grown according to the method of Eimhjellen et al. [17]. Freeze dried *Rps. palustris* was obtained from the American Type Culture Collection (strain ATH 2.1.6) and grown in a culture medium described by Morita and Miyazaki [18]. Both bacteria were harvested separately by centrifugation at $7000 \times g$ for 10 min, washed with 0.025 M Tris (pH 7.5) buffer during the final spin, and stored at −20°C until ready for use. All of the samples utilized in the present work were prepared under a nitrogen atmosphere and contained 0.02 M sodium dithionite, $1.0 \cdot 10^{-5}$ M methyl viologen, 0.05 M glycine (pH 10.1) buffer and 50% ethylene glycol.

Magnetic alignment of the cells was achieved in the dark by placing the sample between the pole faces of a 21 kG magnet and freezing in a liquid nitrogen flowing cryostat. The sample was stored at 77 K in the dark.

EPR measurements were accomplished using a Varian E-109 spectrometer at X-band with 100 kHz field modulation and equipped with an Air Products Helitron cryostat. The triplet states of the bacteria were detected using a light modulation technique similar to that used by other authors [19,20]. The output of the EPR system was fed directly to a Princeton Applied Research Model 220 lock-in amplifier. The reference signal for the lock-in was taken from a 33.5 Hz chopper.

Excitation of the bacteria into their triplet states was achieved using a tungsten lamp filtered by 5 cm of water and focused through the 75% transmitting grid of a Varian TM_{110}(E-238) microwave cavity. Light intensity was

kept below 25 mW/cm^2. Experiments were done routinely at 11 K, and no temperature dependence of the ratios given in Table I was observed up to 20 K. Microwave power was kept below the saturation level.

Finally, because the experimental signals shown in Figs. 2 and 3 are distorted in field position and in intensity owing to sweeping the recorder too quickly, the signal amplitudes used in the computer simulations were not taken from these spectra. Instead, the amplitudes were measured by dialing the magnetic field to coincide with the signal positions and recording the peak heights after a sufficient time for the signals to reach the maximum level. Because the pairs of measured signal intensities were found to be the same within experimental error, the values for the amplitudes are hereafter designated $X^{\pm}$, $Y_1^{\pm}$, $Y_2^{\pm}$ and $Z^{\pm}$.

Results and Discussion

Theoretical model of triplet state EPR

The Hamiltonian matrix for the triplet state in the zero-field basis is given in the usual form [21].

$$\mathcal{H} = \begin{array}{c} \\ \langle T_x| \\ \langle T_y| \\ \langle T_z| \end{array} \begin{array}{c} \begin{array}{ccc} |T_x\rangle & |T_y\rangle & |T_z\rangle \end{array} \\ \begin{bmatrix} X & -ig\beta H_z & ig\beta H_y \\ ig\beta H_z & Y & -ig\beta H_x \\ -ig\beta H_y & ig\beta H_x & Z \end{bmatrix} \end{array} \tag{1}$$

where

$$\begin{aligned} |T_x\rangle &= \frac{1}{\sqrt{2}}|\beta\beta - \alpha\alpha\rangle \\ |T_y\rangle &= \frac{i}{\sqrt{2}}|\beta\beta + \alpha\alpha\rangle \\ |T_z\rangle &= \frac{1}{\sqrt{2}}|\alpha\beta + \beta\alpha\rangle \end{aligned} \tag{2}$$

and X, Y, and Z are the principal values of the spin-dipolar interaction tensor. These quantities are related to the two independent spin parameters $|D|$ and $|E|$ by the equations

$$\begin{aligned} X &= \tfrac{1}{3}|D| + |E| \\ Y &= \tfrac{1}{3}|D| - |E| \\ Z &= -\tfrac{2}{3}|D|. \end{aligned} \tag{3}$$

The eigenstates and eigenvalues of $\mathcal{H}$ are clearly dependent upon the orientation of the static EPR field in the principal axis system of the triplet. Once this orientation is specified, the Hamiltonian can be diagonalized numerically to obtain the wavefunctions and energy levels of the system.

Because the experiments were performed in the high-field limit ($|g\beta H| >> |D|, |E|$), one expects the eigenstates of $\mathcal{H}$ to be close to the high-field eigen-

states

$$|T_{+1}\rangle = |\alpha\alpha\rangle$$
$$|T_0\rangle = \frac{1}{\sqrt{2}}|\alpha\beta + \beta\alpha\rangle \tag{4}$$
$$|T_{-1}\rangle = |\beta\beta\rangle.$$

The eigenstates of $\mathcal{H}$ can be expressed as linear combinations of the zero-field states. The appropriate linear combinations depend upon the orientation of the stated EPR field, H in the principal axis system. Qualitatively, the components

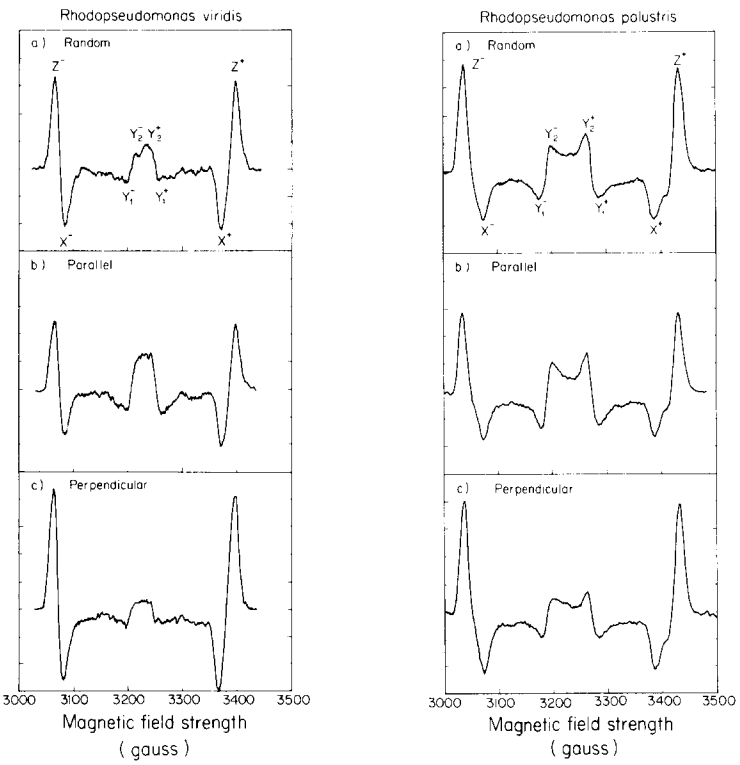

Fig. 2. ***Rps. viridis*** **experimental triplet state spectra. (a) Spectra of randomly ordered, chemically reduced whole cells were taken with the following conditions: sweep time, 8 min; modulation frequency, 100 kHz; modulation amplitude, 16 G; receiver gain, 32; temperature, 11 K; microwave power, 10 μW; microwave frequency, 9.077 GHz; light modulation frequency, 33.5 Hz; recorder time constant, 3 s. (b) Spectra taken with the static EPR field parallel to the alignment field. The other conditions are the same as (a). (c) Spectra taken with the static EPR field perpendicular to the alignment field. The other conditions are the same as (a).**

Fig. 3. ***Rps. palustris*** **experimental triplet state spectra. (a) Spectra of randomly ordered, chemically reduced whole cells were taken with the following conditions: sweep time, 8 min; modulation frequency, 100 kHz; modulation amplitude, 16 G; receiver gain, 63; temperature, 11 K; microwave power, 10 μW; microwave frequency, 9.077 GHz; light modulation frequency, 33.5 Hz; recorder time constant, 3 s. (b) Spectra taken with the static EPR field parallel to the alignment field. The other conditions are the same as (a). (c) Spectra taken with the static EPR field perpendicular to the alignment field. The other conditions are the same as (a).**

of the $|T_0\rangle$ state depend upon the projection of H onto the x, y and z magnetic axes, e.g. if $H \parallel x$, then $|T_0\rangle = |T_x\rangle$, etc.

When H is not precisely along a magnetic axis, one obtains three energy levels close to $|T_{+1}\rangle$, $|T_0\rangle$ and $|T_{-1}\rangle$ designated $|T_\alpha\rangle$, $|T_\beta\rangle$ and $|T_\gamma\rangle$. This designation is structured so that $E_\alpha \approx E_{+1}$, $E_\beta \approx E_0$ and $E_\gamma \approx E_{-1}$, and it will be generally true that as a consequence of the high-field approximation $|E_\beta - E_\alpha|$, $|E_\beta - E_\gamma| \approx |g\beta H|$ for all orientations. Ultimately the eigenstates are expressed as

$$|T_i\rangle = \sum_j |T_j\rangle\, c_j^i \tag{5}$$

$i = \alpha, \beta, \gamma$; $j = x, y, z$, where c_j^i are the eigenvector coefficients, which come from the diagonalization of the Hamiltonian Matrix (Eqn. 1).

Because the triplet state being considered is formed by a radical pair mechanism [11], at high magnetic fields the light-induced triplet is assumed to be populated in the $|T_\beta\rangle$ spin sublevel exclusively. This assumption is consistent with the spin polarization pattern of the observed triplet state spectra (see Figs. 2 and 3), which have been discussed in great detail by many authors [11,20, 22].

The effects of triplet state deactivation are incorporated via a simplified version of the models described by Winscom [23] and Levanon and Vega [24]. Their kinetic equation for the triplet sublevel populations as a function of time is

$$\frac{dn}{dt} = -\hat{k} \cdot n + A \tag{6}$$

where

$$n = \begin{bmatrix} n_\alpha \\ n_\beta \\ n_\gamma \end{bmatrix} \tag{7}$$

gives the steady state populations of the three triplet spin sublevels,

$$A = \begin{bmatrix} A_\alpha \\ A_\beta \\ A_\gamma \end{bmatrix} \tag{8}$$

represents the populating rates of the three sublevels, and

$$\hat{k} = \begin{bmatrix} k_\alpha + W_{\alpha\beta} + W_{\alpha\gamma} & W_{\alpha\beta} & W_{\alpha\gamma} \\ W_{\beta\alpha} & k_\beta + W_{\beta\gamma} + W_{\beta\alpha} & W_{\beta\gamma} \\ W_{\gamma\alpha} & W_{\gamma\beta} & k_\gamma + W_{\gamma\alpha} + W_{\gamma\beta} \end{bmatrix} \tag{9}$$

where k_α, k_β and k_γ are the rate constants for intersystem crossing between the triplet sublevels and the ground state, and the W's are the rate constants for spin-lattice relaxation between the triplet spin sublevels.

If only the $|T_\beta\rangle$ level is populated in the light-modulated generation of the triplet state, one can set $A_\beta = A_0 \sin(\omega t)$ and $A_\alpha = A_\gamma = 0$, where ω is the frequency of light modulation. The intersystem rate constants can be expressed

as

$$k_i = \sum_i |c_j^i|^2 \, k_j \tag{10}$$

$i = \alpha, \beta, \gamma$

$j = x, y, z$

where the k_x, k_y and k_z values can be determined experimentally [24,25] (e.g. by optical detection of magnetic resonance), or by computer simulation (see below). The absence of a temperature dependence of the triplet spectrum in the temperature region in which the experiments were performed and the observation of substantial spin polarization indicate that spin-lattice relaxation is of negligible importance. It is assumed hereafter that k_x, k_y and $k_z >> W_{ij}$, and therefore $W_{ij} = 0$ in Eqn. 9.

A simplified set of differential equations is now obtained. These are

$$\frac{dn_\alpha}{dt} = -k_\alpha n_\alpha \tag{11}$$

$$\frac{dn_\beta}{dt} = -k_\beta n_\beta + A_0 \sin(\omega t) \tag{12}$$

$$\frac{dn_\gamma}{dt} = -k_\gamma n_\gamma . \tag{13}$$

These are easily solved to yield an expression for the population difference between two of the levels. Neglecting exponential terms that will average to zero in the next step, the result in the limit of low microwave power is

$$\Delta n_+ = (n_\beta - n_\alpha) \approx n_\beta \tag{14}$$

$$\Delta n_- = (n_\beta - n_\gamma) \approx n_\beta \tag{15}$$

$$\Delta n_+ = \Delta n_- = \frac{A_0 \sin(\omega t + \phi)}{(\omega^2 + k_\beta^2)^{1/2}} \tag{16}$$

where ϕ is the phase difference between the reference and detector signals. In the light modulation experiment the reference signal given by $R = B \sin(\omega t)$ multiplies Eqn. 16 and averages over time. Furthermore, because $k_\beta >> \omega$ (a chopper frequency of 33.5 Hz is used and k values for similar bacterial systems are known to be at least an order of magnitude larger [2]) one obtains

$$\Delta \bar{n}_\pm = \frac{\omega}{2\pi k_\beta} \int_0^{2\pi/\omega} A_0 \sin(\omega t + \phi) \, B \sin(\omega t) \, dt \tag{17}$$

Adjusting the phase difference between the reference and detector signals to be zero (i.e. $\phi = 0$) and integrating, Eqn. 17 reduces to

$$\Delta \bar{n}_\pm = \frac{C}{k_\beta} \tag{18}$$

where C is a constant term.

Thus each discrete orientation yields two transitions, one in emission and

one in absorption. Since the EPR intensity, I, of a transition is proportional to the population difference, $\Delta n_{\pm}$, the calculated amplitudes are weighted by the inverse of the intersystem crossing rate, k_{β}, which depends upon the contributions of k_x, k_y and k_z to k_{β}, as described in Eqn. 10.

Triplet state EPR from a randomly ordered ensemble

The experimental EPR intensity at a particular static EPR field, $|H|$, is an ensemble average of the triplet signals from all possible orientations of the magnetic system. For a randomly oriented ensemble we have

$$\bar{I}(|H|) \propto \int_0^{\pi/2} \int_0^{\pi/2} I(\theta, \phi, |H|) \sin\theta \, d\theta \, d\phi \tag{19}$$

where $I(\theta, \phi, |H|)$ is the intensity of the triplet signal at field $|H|$ when the static EPR field is specified by the angles θ and ϕ in the principal axis system of the triplet. From the previous section two transitions with energies ϵ_1 and ϵ_2 are obtained by diagonalizing the triplet Hamiltonian matrix (Eqn. 1) with H_x, H_y and H_z determined by θ and ϕ. The intensity is

$$I(\theta, \phi, |H|) \propto \frac{1}{k_{\beta}(\theta, \phi, |H|)} \{\exp[-(\epsilon_1 - |H|)^2/\delta^2] - \exp[-(\epsilon_2 - |H|)^2/\delta^2]\} \tag{20}$$

where it is assumed that each transition has a gaussian profile with line width δ, and the intensity associated with ϵ_2 is negative because this transition is in emission.

The overall spectral lineshape depends upon the zero-field splitting parameters, $|D|$ and $|E|$, and the intersystem crossing rates, k_x, k_y and k_z. When these are known, Eqn. 20 can be evaluated numerically at many field positions to simulate the triplet spectrum.

Simulation of random triplet state spectra

The $|D|$, $|E|$, k_x, k_y and k_z parameters were adjusted to obtain the best fit to the random state spectra of *Rps. viridis* and *Rps. palustris*. This was accomplished by measuring the amplitudes of the triplet signals at a number of key

TABLE I

EXPERIMENTAL AMPLITUDE RATIOS

$Z^{\pm}$, $X^{\pm}$, $Y_1^{\pm}$ and $Y_2^{\pm}$ refer to the amplitudes (in arbitrary units) of the triplet peaks as defined in Materials and Methods. The errors represent the range of possible values for the ratios as deduced from the repeatability of the amplitude measurements.

	$Z^{\pm}/X^{\pm}$	$Z^{\pm}/Y_1^{\pm}$	$Z^{\pm}/Y_2^{\pm}$
Rps. viridis			
Random	−1.6 ± 0.1	−5.8 ± 1.0	5.8 ± 1.0
Parallel	−1.2 ± 0.1	−4.1 ± 0.7	2.5 ± 0.3
Perpendicular	−1.7 ± 0.1	−9.6 ± 1.7	9.6 ± 1.7
Rps. palustris			
Random	−2.1 ± 0.1	−3.6 ± 0.3	4.2 ± 0.4
Parallel	−1.8 ± 0.2	−2.5 ± 0.2	2.5 ± 0.2
Perpendicular	−2.2 ± 0.1	−4.7 ± 0.5	6.1 ± 0.8

TABLE II

ZERO-FIELD SPLITTING PARAMETERS AND RELATIVE RATE CONSTANTS FOR INTERSYSTEM CROSSING

The $|D|$ and $|E|$ zero-field splitting parameters are given in cm^{-1} units. k_x, k_y and k_z refer to rate constants for depopulation of the triplet spin sublevels associated with the $X^{\pm}$, $Y^{\pm}$ and $Z^{\pm}$ triplet peaks as defined in Materials and Methods. The errors in the $|D|$ and $|E|$ values are calculated from the repeatability of the signal position determinations. The errors in the rate constants amount to no more than ± 0.5 and arise from the range of acceptable k values which fit the random spectrum.

	$\|D\|$	$\|E\|$	$k_x : k_y : k_z$
Rps. viridis	0.0153 ± 0.0002	0.0037 ± 0.0002	7.5 : 10.0 : 1.0
Rps. palustris	0.0183 ± 0.0002	0.0035 ± 0.0002	9.0 : 6.0 : 1.0

field positions (see Figs. 2 and 3), calculating ratios, R_E, of these amplitudes (see Table I) and fitting the theoretical spectrum to these ratios.

As a general procedure the $|D|$ parameter was fit first by adjusting it to agree with the separation between the Z^+ and Z^- outermost peak positions (Figs. 2

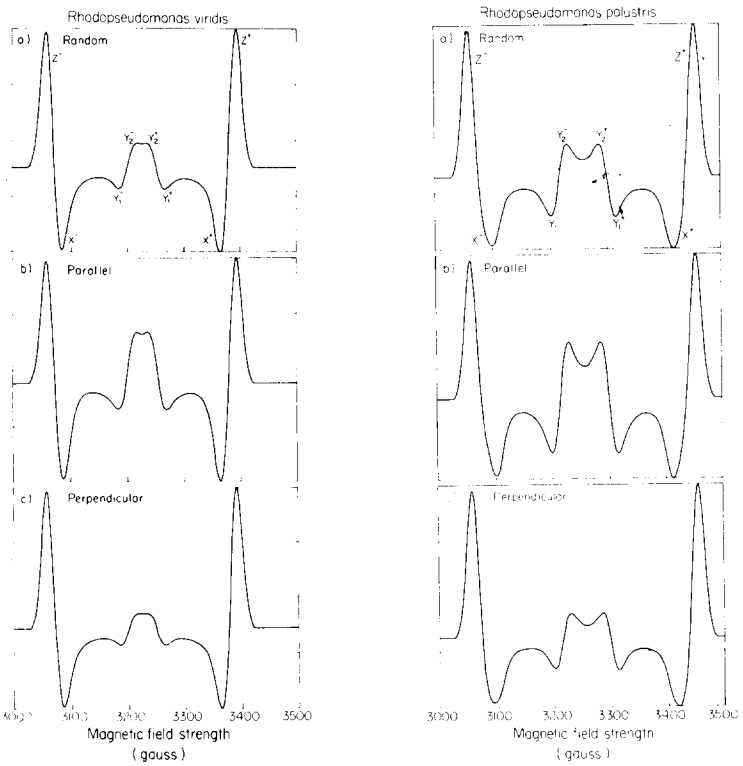

Fig. 4. *Rps. viridis* computer-simulated triplet state spectra assuming (a) random; (b) parallel, and (c) perpendicular orientations of the static EPR field direction with respect to the alignment field direction. Spectra are normalized to the $|Z^-| + |X^-|$ peak amplitudes.

Fig. 5. *Rps. palustris* computer-simulated triplet state spectra assuming (a) random; (b) parallel, and (c) perpendicular orientations of the static EPR field directions with respect to the alignment field direction. Spectra are normalized to the $|Z^-| + |X^-|$ peak amplitudes.

and 3). Then the $|E|$ value was adjusted to the positions of the X^-, Y_1^-, X^+ and Y_1^+ peaks, and the k_x and k_y values were fit to the experimental $Z^\pm/X^\pm$ and $Z^\pm/Y_1^\pm$ ratios, respectively. Because there is some experimental uncertainty in determining the field corresponding to Y_1^- and Y_1^+, the Y_2^- and Y_2^+ amplitudes were used as checks on the E parameter. The parameters that best fit the random triplet state spectra of *Rps. viridis* and *Rps. palustris* are given in Table II. Calculated spectra are displayed in Figs. 4a and 5a.

Triplet state EPR from partially ordered ensembles

Our approach to the calculation of the triplet state EPR spectrum of a partially ordered ensemble is to determine a distribution function, $D(\theta, \phi)$, specifying the probability that a member of the ensemble has a static EPR field direction whose orientation in the principal axis system of the triplet is between θ and $\theta + d\theta$, ϕ and $\phi + d\phi$. The EPR intensity given by Eqn. 19 now becomes

$$\bar{I}(|H|) = \int_0^{2\pi} \int_0^{\pi} I(\theta, \phi, |H|) D(\theta, \phi)\, d\theta\, d\phi. \tag{21}$$

The details of the method of calculation of $D(\theta, \phi)$ are presented in a separate publication [26] which treats both the general case and the specific one of magnetically aligned *Rps. viridis* cells. In the present paper the derivation of $D(\theta, \phi)$ will be discussed qualitatively and the interested reader is referred to reference [26] for a mathematically rigorous approach.

As discussed previously the bacteria used in these experiments are approximately prolate ellipsoids (see Fig. 1). The internal membranes form concentric, roughly cylindrical sheets having a common axis with the longitudinal axis of the cell. The reaction center particles, which contain the paramagnetic species giving rise to the light-induced triplet state spectra, are imbedded in these membranes.

Three axis systems which will be useful in characterizing the distribution of the magnetic systems are now defined (see Fig. 1):

(1) The laboratory axis system is one in which the static EPR field has fixed components. The orientation of various members of the ensemble of spin systems is specified with respect to this fixed reference frame.

(2) The principal magnetic axis system is the coordinate system in which the dipolar Hamiltonian $\mathcal{H} = \boldsymbol{S} \cdot \hat{D} \cdot \boldsymbol{S}$ is diagonal. It is related to the intermediate axis system by a fixed set of Euler angles, α', β' and γ'.

(3) The intermediate axis system serves as a bridge between the laboratory frame and the principal magnetic axis system. One can think of the magnetic system as being enclosed in a cube. The unit vectors of the intermediate axis system lie along three joined edges of the cube. The magnetic system is fixed within the cube, so that an Euler rotation matrix, $A(\alpha', \beta', \gamma')$, will bring the magnetic axis system into coincidence with the intermediate axis. This transformation is the same for every member of the ensemble.

The ensemble of magnetic systems is generated by performing a set of symmetry operations on an intermediate axis system which is initially superimposed on the laboratory axis system. These symmetry operations can be

derived from a consideration of the orienting process and the morphology of the organism. The ensemble so generated is an ensemble of intermediate axis systems. It will be necessary later to transform to the principal axis system.

As mentioned before, the 21 kG magnetic field axis aligns the cells so that their longitudinal axes lie in a plane normal to the alignment field. Because this is the only restriction, there are still two symmetry operations which can be performed on the cells; rotation χ about the alignment field and rotation μ about the longitudinal axis of the cell. These operations are illustrated in Fig. 1.

Linear dichroism [15], photoselection [16], and the present experiments suggest that the reaction center particles are highly ordered within the membranes. A convenient and physically reasonable convention is that the membrane surface defines a unique axis normal to it. This analysis hypothesizes a random distribution of intermediate axis systems about this direction and therefore generates a third symmetry operation λ (see Fig. 1). The theoretical analysis is greatly facilitated by choosing the membrane normal to be coincident with the z-axis of the intermediate axis system.

If the above ordering were perfect, i.e. the cells were perfect ellipsoids, the membranes perfect cylinders, the alignment in the magnetic field complete, and the unique reaction center particle axis always 0° from the normal, it would be easy to generate the ensemble from the above symmetry operations. However, it is necessary to take into account deviations from these conditions. The most significant deviations are likely to be imperfections in the cell shape and membrane surface. This can be described by a tilt of the membrane normal from the perfect cylinder normal. We call this tilt the wobble angle, w, (see Fig. 1).

The imperfections introduce some uncertainty into the value of this angle. This problem is treated phenomenologically by defining a distribution function, $g(w)$, which gives the probability that a member of the ensemble has a particular wobble, w. For the calculation this function is taken to be a Gaussian

$$g(w) = \cos w \exp(-w^2/\Delta^2) \tag{22}$$

where 1.7Δ equals the full width at half-maximum and is hereafter referred to as the disorder parameter, and the $\cos w$ provides the proper volume element for the integration.

The problem now is to obtain $D(\theta, \phi)$ in Eqn. 21 by a consideration of $g(w)$. It suffices to calculate $D'(\theta', \phi')$, the distribution function of intermediate axis systems having static EPR field components specified by θ' and ϕ'. It is then a simple matter to calculate $D(\theta, \phi)$ of Eqn. 21 from $D'(\theta', \phi')$ using the fixed geometrical relation between the intermediate axis system and the principal axis system. The intuitive way to approach this is to ask the question: given a member of the ensemble with the static EPR field specified by θ' and ϕ', what is the value of w which generated this orientation? Unfortunately, one cannot answer this question directly; because of the three other symmetry operations, w is not uniquely defined by θ' and ϕ'.

This suggests, however, that one could express $D'(\theta', \phi')$ as an integral over $g(w)$ and some other function which gives the probability that the ensemble member was generated via a wobble, w. Such an expression can be obtained by

a formal coordinate transformation. This procedure is outlined by Friesner et al. [26]. The final expressions for the cases of the static EPR field parallel and perpendicular to the alignment field direction are given below.

$$D'_{\parallel}(\theta') = \sin\theta' \int_{\cos w = 1}^{\cos w = \cos\theta'} \left(1 - \frac{\cos^2\theta}{\cos^2 w}\right)^{-1/2} \cdot \frac{g(w)}{\cos w}\, dw \tag{23}$$

$$D'_{\perp}(\theta') = \sin\theta' \int_{0}^{\pi/2} g(w) \cdot G(\theta', w)\, dw \tag{24}$$

where

$$G_{\pm}(\theta', w) = \frac{2}{\sqrt{[1 \pm \sin(\theta' + w)][1 \pm \sin(\theta' - w)]}} K(k_{\pm}) \tag{25}$$

and

$$k_{\pm} = \left\{ \frac{\pm 2[\sin(\theta' - w) + \sin(\theta' + w)]}{[1 \pm \sin(\theta' + w)][1 \pm \sin(\theta' + w)]} \right\}^{1/2} \tag{26}$$

$K(k_{\pm})$ is the complete elliptic integral of the first kind, and

$$G(\theta', w) = \begin{cases} G_{+}(\theta', w) \text{ for } [\sin(\theta' - w) + \sin(\theta' + w)] > 0 \\ G_{-}(\theta', w) \text{ for } [\sin(\theta' - w) + \sin(\theta' - w)] < 0 \end{cases}$$

Note that $D'(\theta')$ has been reduced to an axial form, i.e. depends only on θ'. Intuitively, this is what one would expect, since there is ordering in only one angular parameter, w. Because both $D'_{\parallel}(\theta')$ and $D'_{\perp}(\theta')$ can be evaluated numerically, one can then use Eqn. 21 to simulate the parallel and perpendicular triplet spectra of *Rps. viridis* and *Rps. palustris.*

Simulation of partially ordered triplet state spectra

The results of the previous section give the distribution function for the ensemble of intermediate axis systems. To use Eqn. 21 one needs the probability distribution function in the principal axis system. This is obtained as follows: the static EPR field orientation is characterized by θ and ϕ in the principal axis system. The angle, θ', between the membrane normal and the static EPR field is derived from the relation

$$\cos\theta' = \boldsymbol{n} \cdot \boldsymbol{H}(\theta, \phi) \tag{28}$$

or

$$\theta' = \cos^{-1}[\boldsymbol{n} \cdot \boldsymbol{H}(\theta, \phi)] \tag{29}$$

Then

$$D(\theta, \phi) = \frac{\sin\theta}{\sin\theta'} D'(\theta') = \frac{\sin\theta}{\sin\theta'} D'\{\cos^{-1}[\boldsymbol{n} \cdot \boldsymbol{H}(\theta, \phi)]\} \tag{30}$$

where $[(\sin\theta)/(\sin\theta')]$ is the Jacobian for the transformation of the distribution function from the intermediate axis system to the principal axis system [26].

The variable parameters to be determined in this simulation are the disorder

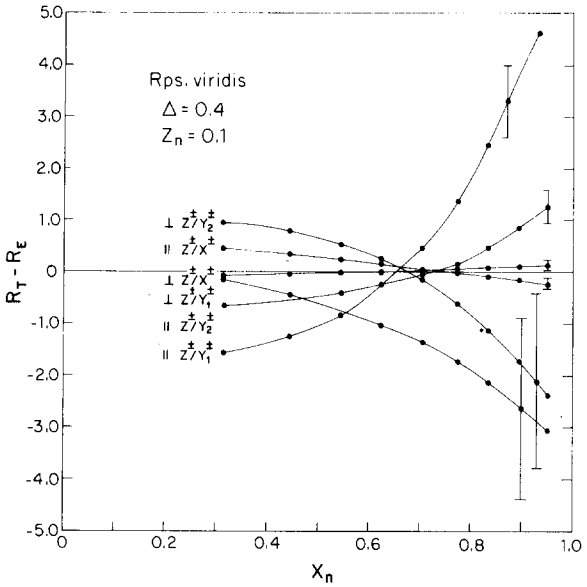

Fig. 6. *Rps. viridis* plots of theoretical amplitude ratio minus experimental amplitude ratio, $R_T - R_E$, versus the projection, X_n, of the x'' principal magnetic axes onto the normal to the membrane for Z_n = 0.10 and Δ = 0.40.

parameter, Δ, (Eqn. 22) and the orientation of the normal to the membrane in the principal axis system. The latter is determined by projections of the normal on the three magnetic axes and designated X_n, Y_n and Z_n (only two of which are independent). The $|D|$, $|E|$, k_x, k_y and k_z values determined by the random simulation were held constant.

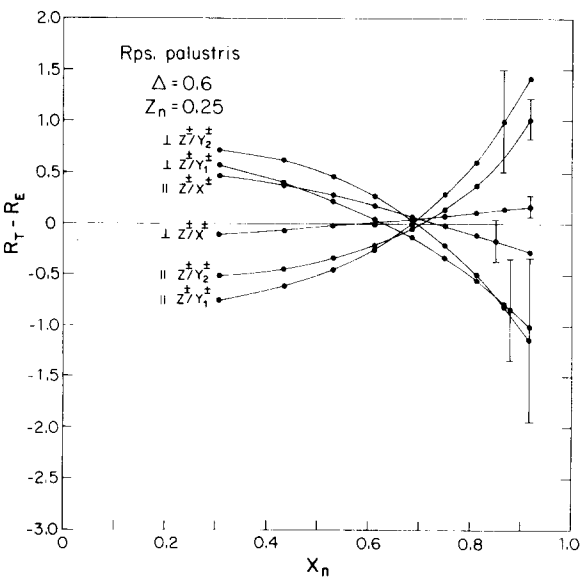

Fig. 7. *Rps. palustris* plots of theoretical amplitude ratio minus experimental amplitude ratio, $R_T - R_E$, versus the projection, X_n, of the x'' principal magnetic axes onto the normal to the membrane for Z_n = 0.25 and Δ = 0.60.

TABLE III

ORIENTATION PARAMETERS FOR THE PRIMARY DONORS IN PHOTOSYNTHETIC BACTERIA

X_n, Y_n and Z_n are the calculated projections of the x'', y'' and z'' principal magnetic axes onto the normal to the membrane. 1.7Δ is the distribution width (in radians) of the 'wobble' angle, w. The values in parentheses are the angles between the normal to the membrane and the principal magnetic axes. They are related to the projections by $\theta_X = \cos^{-1} X_n$, etc. The values were determined by the best fit of the theoretical spectra to the experimental ratios given in Table I.

	X_n	Y_n	Z_n	Δ
Rps. viridis	0.67 (48°)	0.74 (42°)	0.10 (84°)	0.40
Rps. palustris	0.69 (46°)	0.69 (46°)	0.25 (76°)	0.60

The fitting procedure was done as follows: ratios of the experimentally observed amplitudes were calculated for the parallel and perpendicular cases (see Table I). Values for Z_n and Δ were chosen, and plots of the theoretical minus experimental ratios ($R_T - R_E$) vs. X_n were made (see Figs. 6 and 7), X_n being varied between 0.1 and 0.9. Then in a systematic fashion Δ was varied between 0.1 and 1.6, and Z_n was varied between 0.1 and 0.9. A set of parameters was sought for which the graphs indicated $(R_T - R_E) = 0$ within experimental error for all six ratios.

The best solution for *Rps. viridis* is given in Table III. As shown in Fig. 6 all six curves cross zero near $X_n = 0.67$ where $Z_n = 0.10$ and therefore $Y_n = 0.74$. These numbers are easily converted into the angles that the three principal axes make with the normal by the relations $\theta_X = \cos^{-1} X_n$, etc. $\Delta = 0.4$ represents the disorder in the system as defined by Eqn. 22. The calculated spectra for the

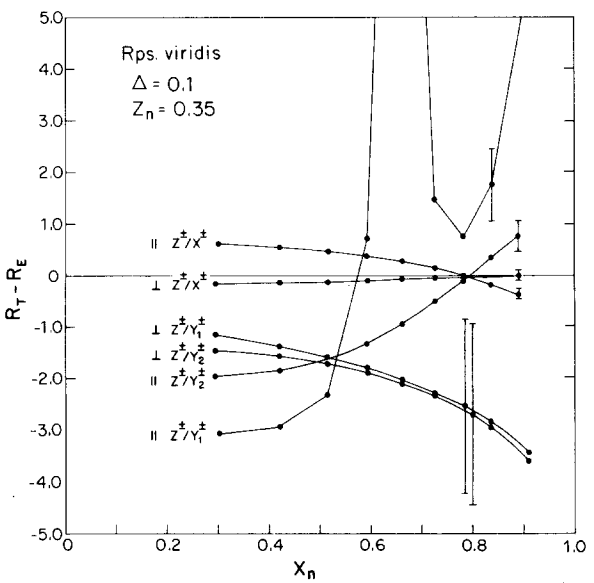

Fig. 8. *Rps. viridis* plots of theoretical minus experimental amplitude ratios versus the projection, X_n, of the x'' principal magnetic axes onto the normal to the membrane for a typical non-solution region (i.e. one lying outside the experimental error).

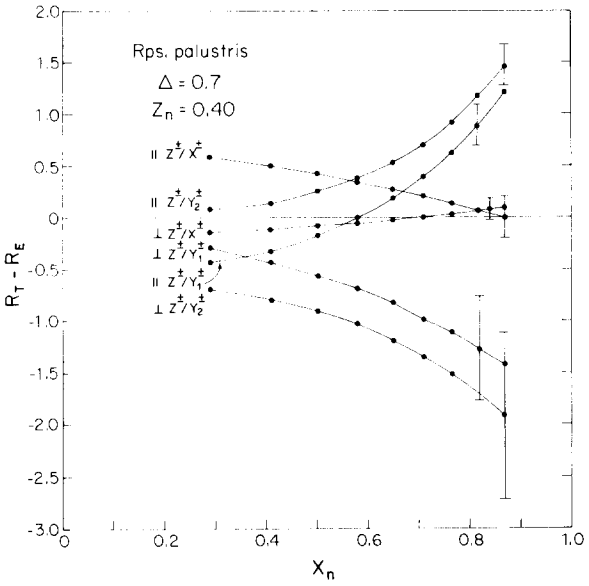

Fig. 9. *Rps. palustris* plots of theoretical minus experimental amplitude ratios versus the projection, X_n, of the x'' principal magnetic axes onto the normal to the membrane for a typical non-solution region (i.e. one lying outside the experimental error).

static EPR field parallel and perpendicular to the alignment field are shown in Fig. 4b and c.

For the *Rps. palustris* organism the solution in Table III indicated a geometry similar to *Rps. viridis*. A larger value for Δ was necessary however, to simulate the *Rps. palustris* triplet state spectra, and this most likely reflects a distortion of the cells away from their ellipsoidal shape. Nevertheless, the spectra were simulated (see Fig. 5b and c), and Fig. 7 shows that $(R_T - R_E) = 0$ for all six ratios for the parameters, $X_n = 0.69$, $Y_n = 0.69$, $Z_n = 0.25$ and $\Delta = 0.6$ given in Table III.

Typical sets of non-solution curves for *Rps. viridis* and *Rps. palustris* are given in Figs. 8 and 9. Clearly, no point along the abscissa provides a solution as previously defined.

Conclusion

A simulation of the random experimental spectra of these triplet states provides an alternate method to those of other groups [24,25,27] for measuring their static and kinetic parameters. The $|D|$ and $|E|$ parameters extracted from this work do not differ appreciably from previous measurements by other groups [5,27]. The kinetic constants for the two species of bacteria have not yet been experimentally determined by other methods. In principle, optical detection of magnetic resonance can provide a more accurate determination of the rate constants. However, there have been serious discrepancies in the values for these decay constants reported by different groups for similar systems [2,27]. Our method provides an independent measurement of the relative values of k_x, k_y and k_z.

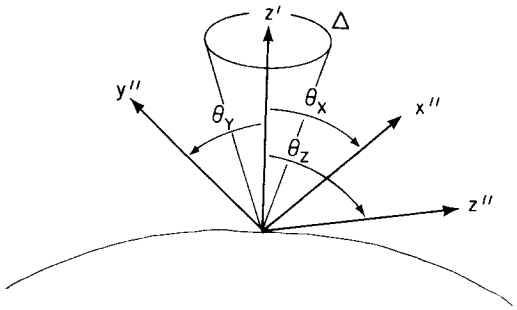

Fig. 10. Orientation of the triplet magnetic axes of the primary donors in *Rps. viridis* and *Rps. palustris* with respect to the cylindrical membrane surface. θ_X, θ_Y, θ_Z and Δ are given in Table III.

It is interesting to note that the kinetic constants extracted from these measurements and given in Table II display a different trend for *Rps. viridis* (i.e. $k_y > k_x > k_z$) than for *Rps. palustris* (i.e. $k_x > k_y > k_z$). The factors controlling these trends are beyond the scope and focus of the present work; they have been dealt with in detail in previous publications [28,29].

Models for the orientation of the triplet magnetic axes of the primary electron donor with respect to the membranes in *Rps. viridis* and *Rps. palustris* are given in Fig. 10. Figs. 2 and 3 show that the effect of orientation on the triplet state spectra for the two organisms is very similar. Therefore, it is not surprising that the calculation yields similar geometries for the triplet magnetic axes in the two species. Perhaps more remarkable is the fact that a unique orientation of the triplet magnetic axes exists in two different bacterial organisms having chemically distinct primary donors.

For both *Rps. viridis* and *Rps. palustris* only one region of the three dimensional space spanned by the three independent parameters, X_n, Z_n and Δ, gave a solution to the orientation problem within experimental error. This region of solution was approximated by a rectangular parallelepiped with boundary conditions given in Table IV. The region of solution was relatively large for *Rps. palustris* since the orientation effect was small. The larger orientation effect in *Rps. viridis* led to a correspondingly smaller region of solution for this organism. The error limits that appear involve the repeatability of the experimental measurements as stated in Table I. Our investigation of the light intensity dependence, microwave power dependence and temperature dependence of the amplitude ratios given in Table I led us to the conclusion that systematic errors from these sources were negligible.

TABLE IV

BOUNDARY CONDITIONS FOR THE REGIONS OF SOLUTION

The regions of solution are given by a rectangular parallelepiped, the dimensions of which are determined by X_n and Z_n which are the projections of the x'' and z'' magnetic axes onto the normal to the membrane, and Δ which is the disorder parameter as defined in the text. No solution outside these regions fell within experimental error.

Rps. viridis	$0.65 < X_n < 0.75$	$0.0 < Z_n < 0.15$	$0.3 < \Delta < 0.5$
Rps. palustris	$0.5 < X_n < 0.7$	$0.0 < Z_n < 0.3$	$0.4 < \Delta < 0.8$

These results represent the first report of an oriented triplet state in photosynthetic systems. It is therefore appropriate to contrast our technique with other methods of extracting orientation information; e.g. linear dichroism. First, our method provides a good quantitative estimate for the degree of disordering of the system; this is reflected in the narrow range of acceptable values for Δ. The determination of the disorder parameter from linear dichroism experiments is much more uncertain [16]. Secondly, we obtain information about the orientation of magnetic axes rather than optical transition moment directions. This information provides an independent set of data which can be used in conjuction with optical measurements to locate the bacteriochlorophyll monomers of the special pair within the membranes.

The problem of the orientation of the dimer pair in the photosynthetic membrane can be divided into two parts:

(1) The relative orientation of the two bacteriochlorophyll monomers. This can be specified by five angles and the center-to-center distance, R_{12}.

(2) Orientation of the dimer pair with respect to the membrane surface. This is specified by three angles.

In this paper we have determined two of the three angles needed to orient the dimer pair in the membrane. The third angle may not be uniform over the ensemble (e.g. if the dimer pair has no preferred orientation about the normal to the membrane). It may be possible to combine our results with the linear dichroism studies to investigate this question more quantitatively.

Our results, in combination with the linear dichroism work, set some conditions on the relative orientation of the two monomers. However, there are not enough independent conditions to determine the six unknown coordinates for this part of the problem. We therefore intend to combine the present work and linear dichroism measurements with circular dichroism and optical detection of magnetic resonance data to obtain a coherent and self-consistent picture of the structure of the reaction center in bacterial photosynthesis. The use of these techniques in combination will over-determine the solution of this very important problem and, therefore, allow us to propose a structure for the relative orientation of the two bacteriochlorophyll monomers with respect to each other and to specify the orientation of the dimer pair with respect to the membrane in which it resides.

Acknowledgements

The authors wish to thank Mr. John Bolt and Ms. Mary McLean for their help in the bacterial preparations. We also gratefully acknowledge the many enthusiastic and stimulating discussions with Dr. Jacques Breton. This research was supported in part by the Biomedical and Environmental Research Division of the US Department of Energy, by National Science Foundation Grant PCM 76-5074, a NIH National Research Service Award to H.A.F. and a University of California Regents Fellowship to J.A.N.

References

1 Levanon, H. and Norris, J.R. (1978) Chem. Rev. 78, 185—198

2 Clarke, R.H., Connors, R.E. and Frank, H.A. (1976) Biochem. Biophys. Res. Commun. 71, 671—675

3 Clarke, R.H., Connors, R.E., Frank, H.A. and Hoch, J.C. (1977) Chem. Phys. Lett. 45, 523—528
4 Leigh, J.S. and Dutton, P.L. (1974) Biochim. Biophys. Acta 357, 67—77
5 Prince, R.C., Leigh, J.S. and Dutton, P.L. (1976) Biochim. Biophys. Acta 440, 622—636
6 Prince, R.C., Tiede, D.M., Thornber, J.P. and Dutton, P.L. (1977) Biochim. Biophys. Acta 462, 467—490
7 McElroy, J.D., Feher, G. and Mauzerall, D.C. (1972) Biochim. Biophys. Acta 267, 363—374
8 Norris, J.R., Scheer, H., Druyan, M.B. and Katz, J.J. (1974) Proc. Natl. Acad. Sci. U.S. 71, 4897—4900
9 Feher, G., Hoff, A.J., Isaacson, R.A. and Ackerson, L.C. (1975) Ann. N.Y. Acad. Sci. 244, 239—259
10 Parson, W.W. and Monger, T.G. (1977) Brookhaven Symp. Biol. 28, 195—211
11 Blankenship, R.E. and Parson, W.W. (1979) in Topics in Photosynthesis (Barber, J., ed.), Vol. 3., pp. 71—114, Elsevier, Amsterdam
12 Giesbrecht, P. and Drews, G. (1966) Arch. Mikrobiol. 54, 297—330
13 Tauschel, H.-D. and Drews, G. (1967) Arch. Mikrobiol. 59, 381—404
14 Oelze, J. and Drews, G. (1972) Biochim. Biophys. Acta 265, 209—239
15 Breton, J. (1974) Biochem. Biophys. Res. Commun. 59, 1011—1017
16 Paillotin, G., Vermeglio, A. and Breton, J. (1979) Biochim. Biophys. Acta 545, 249—264
17 Eimhjellen, K.E., Aasmundrud, O. and Jensen, A. (1963) Biochem. Biophys. Res. Commun. 10, 232—236
18 Morita, S. and Miyazaki, T. (1971) Biochim. Biophys. Acta 245, 151—159
19 Norris, J.R., Uphaus, R.A. and Katz, J.J. (1975) Chem. Phys. Lett. 31, 157—161
20 Thurnauer, M.C., Katz, J.J. and Norris, J.R. (1975) Proc. Natl. Acad. Sci. U.S. 72, 3270—3274
21 Carrington, A. and McLachlan, A.D. (1967) Introduction to Magnetic Resonance, p. 119, Harper and Row, New York
22 Kleibeuker, J.F., Platenkamp, R.F. and Schaafsma, T.J. (1976) Chem. Phys. Lett. 41, 557—561
23 Winscom, C.J. (1975) Z. Naturforsch. 30a, 571—582
24 Levanon, H. and Vega, S. (1974) J. Chem. Phys. 61, 2265—2274
25 Clarke, R.H. and Hofeldt, R.H. (1974) J. Chem. Phys. 61, 4582—4587
26 Friesner, R., Nairn, J.A. and Sauer, K. (1978) J. Chem. Phys., in the press
27 Hoff, A.J. and Gorter de Vries, H. (1979) Biochim. Biophys. Acta 503, 94—106
28 Clarke, R.H., Connors, R.E., Schaafsma, T.J., Kleibeuker, J.F. and Platenkamp, R.J. (1976) J. Am. Chem. Soc. 98, 3674—3677
29 Clarke, R.H. and Frank, H.A. (1977) Chem. Phys. Lett. 51, 13—17